

analyzed by RNase protection assay, was present in all brain compartments examined (22). Approximate extracellular IFN- $\gamma$  production by recombinant virus is  $1.5 \times 10^6$  plaque-forming units (pfu) per unit of IFN- $\gamma$ , as determined by L-929 bioactivity assay. The relative roles of secreted and intracellular IFN- $\gamma$  in SV clearance are unclear, but previous studies have shown that intracellular IFN- $\gamma$  can mediate virus protection in an IFN- $\gamma$  receptor-dependent fashion similar to that of exogenous IFN- $\gamma$  (23). Therefore, local production of IFN- $\gamma$  alone is sufficient to effect T cell-mediated clearance of virus from some, but not all regions of the CNS. IFN- $\gamma$  has direct antiviral activity in peripheral tissues and is important for clearance of mouse hepatitis virus from neurons and of VV from choroidal and meningeal cells in vivo (21, 24, 25). Our data provide further evidence for the specific role of IFN- $\gamma$  in noncytolytic clearance of virus from some, but not all, types of neurons.

CD8 T cells function through cytokine production and/or the cytotoxic response. It is widely accepted that cytotoxic T lymphocytes (CTL) provide antiviral protection through lysis of infected cells (26). However, in situations where the cells are nonrenewable or where large numbers of cells are infected, lysis is counterproductive or not effective. Early studies of persistent lymphocytic choriomeningitis virus infection of the CNS suggested that CD8 T cells could resolve infection without necrosis (27), and evidence has accumulated for alternate noncytolytic, cytokine-mediated T cell mechanisms of virus clearance (6, 28, 29). Our study demonstrates IFN- $\gamma$ -mediated noncytolytic clearance of virus from neurons in vivo, providing evidence for the role of T cell cytokine production in the resolution of virus infection as an alternative to CTL-mediated killing of virus-infected cells. However, neurons are heterogeneous in their responses to IFN- $\gamma$ , resulting in a failure to contain virus replication in localized regions of the CNS. These results define some of the important immune components for recovery from viral encephalomyelitis, which could be useful in developing therapies targeted for specific regions of the CNS.

References and Notes

1. A. C. Jackson, T. R. Moench, B. D. Trapp, D. E. Griffin, *Lab. Invest.* **58**, 503 (1988).
2. D. E. Griffin, R. T. Johnson, *J. Immunol.* **118**, 1070 (1977).
3. B. Levine *et al.*, *Science* **254**, 856 (1991).
4. S. L. Wesselingh, D. E. Griffin, *J. Immunol.* **152**, 1289 (1994).
5. L. G. Guidotti, F. V. Chisari, *Virology* **273**, 221 (2000).
6. L. G. Guidotti *et al.*, *Science* **284**, 825 (1999).
7. A. J. Ramsay, J. Ruby, I. A. Ramshaw, *Immunol. Today* **14**, 155 (1993).
8. E. Joly, L. Mucke, M. B. A. Oldstone, *Science* **253**, 1283 (1991).
9. T. Kimura, D. E. Griffin, *J. Virol.* **13**, 6117 (2000).

10. D. Kitamura, J. Roes, R. Kuhn, K. Rajewsky, *Nature* **350**, 423 (1991).
11. P. C. Tucker, D. E. Griffin, *J. Virol.* **65**, 1551 (1991).
12. Wild-type C57BL/6J, antibody knockout C57BL/6-*Igh-6<sup>tm1Cgn</sup>*, SCID C57BL/6J-*Prkdc<sup>scid</sup>/Szj*, and recombination activating gene-1 knockout C57BL/6J-*Rag1<sup>tm1Mom</sup>* were purchased from the Jackson Laboratory at 4 to 6 weeks of age. For infection, 1000 pfu of SV in 30  $\mu$ l of Hanks' balanced salt solution was injected intracerebrally with a tuberculin syringe.
13. The Web figures are available on Science Online at [www.sciencemag.org/cgi/content/full/293/5528/303/DC1](http://www.sciencemag.org/cgi/content/full/293/5528/303/DC1).
14. The GK1.5 ( $\alpha$ -CD4)- and 2.43 ( $\alpha$ -CD8)-producing hybridomas (American Type Culture Collection, Manassas, VA) were injected into SCID mice for ascites production, and antibody was quantitated by enzyme-linked immunosorbent assay (Bethyl Laboratories). Mice were given 0.25 mg of antibody in a total of 0.5 ml of phosphate-buffered saline intraperitoneally every day for 3 days. Three days later, depletion was complete (>98%) and mice were infected with SV. Depletion was confirmed for each mouse by flow cytometric analysis of spleen cells.
15.  $\mu$ MT mice were vaccinated in each footpad with either 330 pfu of SV or  $2.5 \times 10^4$  pfu of VV. Six days later, lymphocytes from draining lymph nodes were removed and suspended in Dulbecco's modified essential medium containing 10% fetal bovine serum and penicillin or streptomycin. SCID mice were infected with SV 3 days before intraperitoneal transfer of  $6 \times 10^6$  cells.
16. J. P. Kelly, in *Principles of Neural Science*, E. R. Kandel, J. H. Schwartz, T. M. Jessell, Eds. (Elsevier Science, New York, 1991), pp. 283–295.
17. ———, J. Dodd, in *Principles in Neural Science*, E. R. Kandel, J. H. Schwartz, T. M. Jessell, Eds. (Elsevier Science, New York, 1991), pp. 273–282.
18. L. Schnell, S. Fearn, H. Klassen, M. E. Schwab, V. H. Perry, *Eur. J. Neurosci.* **11**, 3648 (1999).
19. L. P. McCluskey, L. Lampson, *J. Neuropathol. Exp. Neurol.* **59**, 177 (2000).
20. E. H. Cheng, B. Levine, L. H. Boise, C. B. Thompson, J. M. Hardwick, *Nature* **379**, 554 (1996).
21. B. D. Pearce, M. V. Hobbs, T. S. McGraw, M. J. Buchmeier, *J. Virol.* **68**, 5483 (1994).
22. G. K. Binder, D. E. Griffin, unpublished data.
23. A. Will, U. Hemmann, F. Horn, M. Rollinghoff, A. Gessner, *J. Immunol.* **157**, 4576 (1996).
24. M. Lin, D. Hinton, S. Stohlmann, *Adv. Exp. Med. Biol.* **440**, 431 (1998).
25. T. M. Kundig, H. Hengartner, R. M. Zinkernagel, *J. Immunol.* **150**, 2316 (1993).
26. R. M. Zinkernagel, P. C. Doherty, *Nature* **248**, 701 (1974).
27. M. B. A. Oldstone, P. Blount, P. J. Southern, *Nature* **321**, 239 (1986).
28. I. A. Ramshaw *et al.*, *Immunol. Rev.* **159**, 119 (1997).
29. L. G. Guidotti *et al.*, *Immunity* **4**, 25 (1996).
30. We thank B. Schofield for assistance in imaging and photography. Supported by grants from the Markey Foundation (G.K.B.) and from the National Institute of Neurological Diseases and Stroke (D.E.G.).

9 February 2001; accepted 30 May 2001

## Homeostatic Regulation of the Immune System by Receptor Tyrosine Kinases of the Tyro 3 Family

Qingxian Lu and Greg Lemke\*

Receptor tyrosine kinases and their ligands mediate cell-cell communication and interaction in many organ systems, but have not been known to act in this capacity in the mature immune system. We now provide genetic evidence that three closely related receptor tyrosine kinases, Tyro 3, Axl, and Mer, play an essential immunoregulatory role. Mutant mice that lack these receptors develop a severe lymphoproliferative disorder accompanied by broad-spectrum autoimmunity. These phenotypes are cell nonautonomous with respect to lymphocytes and result from the hyperactivation of antigen-presenting cells in which the three receptors are normally expressed.

The elimination of reactive lymphocytes is a central feature of homeostatic regulation in the immune system. Although clonal expansion of lymphocytes is essential for immune responses, activated T and B cells must be deleted once the antigens that triggered their expansion have been eradicated. Similarly, autoreactive T cell clonotypes pose a severe threat to tissue and organ integrity, and must also be deleted. Deficiencies in the homeostatic regulation of expanded or autoreactive lymphocytes lead to lymphoproliferative dis-

orders, impaired immune function, autoimmunity, and death (1).

In the mature immune system, lymphocyte numbers are under the control of a wide variety of soluble cytokines, as well as cell surface inhibitory and costimulatory molecules. Although many of these regulators bind to receptors that are coupled to cytoplasmic protein-tyrosine kinases (PTKs), none of them is known to signal through the more direct mechanism of binding and activating a receptor with intrinsic PTK activity (2). This notwithstanding, we have found that three structurally related receptor PTKs—Tyro 3 (3, 4), Axl (3, 5), and Mer (3, 6)—play an essential immunoregulatory role. These receptors are, together with their ligands Gas6

Molecular Neurobiology Laboratory, The Salk Institute, La Jolla, CA 92037, USA.

\*To whom correspondence should be addressed. E-mail: [lemke@salk.edu](mailto:lemke@salk.edu)

## REPORTS

and Protein S (7, 8), widely coexpressed in cells of the immune, nervous, vascular, and reproductive systems, but their biological roles in these tissues have only recently begun to be addressed directly (9).

We have analyzed the immune system phenotypes of an allelic series of mice that are singly, doubly, and triply mutant in the *Tyro 3*, *Axl*, and *Mer* genes (9). At birth, even triple mutants of this series displayed peripheral lymphoid organs of normal size and weight, and the initial postnatal development of both their lymphoid and myeloid cell lineages was not obviously different from wild type. Beginning at ~4 weeks, however, the spleens and lymph nodes of these triple mutants grew at elevated rates relative to wild type (Fig. 1, A through C), such that by 1 year of age, their spleen weights were on average 10 times that of wild type (C57Bl/6 × 129sv) (Fig. 1C). Dramatic enlargements of lymph nodes were also evident in all triple mutants, notably in the submaxillary, popliteal, and mesenteric nodal stations (Fig. 1A). These

changes were progressively dependent on the inactivation of all three genes in the *Tyro 3* family (Fig. 1C), a genetic interaction through the allelic series that is consistent with the extensive coexpression of *Tyro 3*, *Axl*, and *Mer* in cells of the immune system and elsewhere (9).

The aberrant growth of peripheral lymphoid organs was primarily due to the hyperproliferation of B and T cells. Although both classes of lymphocyte were greatly increased in the triple mutants, flow cytometric analyses (10) revealed a modest but selective enrichment of T cells over B cells (Fig. 1, D and E). Within T cell populations, we detected a further enrichment for CD4<sup>+</sup> over CD8<sup>+</sup> cells (Fig. 1E). The continued proliferation of B and T cells in the triple mutants eventually filled their lymphoid compartments beyond capacity. Remarkably, we detected ectopic colonies of lymphocytes in every adult organ that we examined, including lung, liver, kidney, heart, pancreas, intestine, skeletal muscle, eye, brain, and spinal cord (Fig. 1, F and G).

The B and T cell populations of the triple

mutants were also constitutively activated. Elevated numbers of triple mutant T cells, for example, expressed the interleukin-2 (IL-2) receptor (Fig. 2A) and the lectin CD69 (11), both markers of T cell activation. Similarly, triple mutant B cells displayed elevated surface expression of the acute activation marker Fas (Fig. 2B) and the chronic activation marker CD44 (Fig. 2C), and a pronounced increase in the expression of interferon-gamma (IFN- $\gamma$ ) was observed in the spleen and lymph nodes (Fig. 2D). The broad activation of B and T cells was, in turn, reflected in the activation of nonimmune tissues with which these cells interact. For example, intercellular adhesion molecule-1 (ICAM-1), which is required for lymphocyte adhesion to blood vessels and subsequent invasion of tissue parenchyma, was strongly up-regulated in the vascular endothelia of the triple mutants (Fig. 2E).

All triple mutants eventually developed autoimmunity. Disease symptoms, which were first detectable in a subset of individuals at ~4 weeks after birth, were histologically similar to those seen in a broad spectrum of

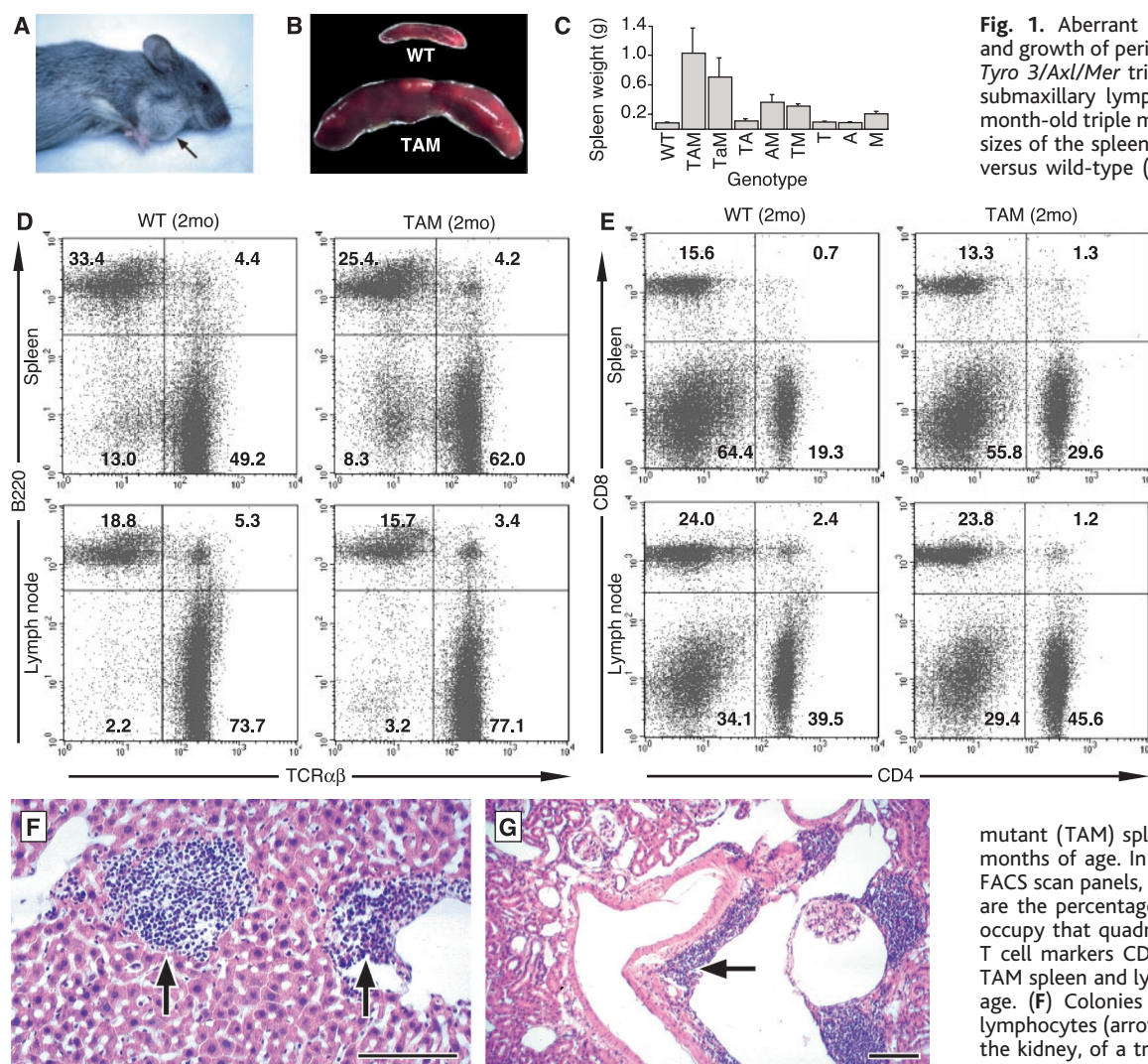


**Fig. 1.** Aberrant lymphocyte proliferation and growth of peripheral lymphoid organs in *Tyro 3/Axl/Mer* triple mutants. (A) Enlarged submaxillary lymph node (arrow) in a 10-month-old triple mutant female. (B) Relative sizes of the spleen in a triple mutant (TAM) versus wild-type (WT) male at 1 year. (C)

Adult spleen weight as a function of genotype. T, A, and M represent *Tyro 3*, *Axl*, and *Mer* single mutants, and so forth. TM represents *Tyro 3/Mer* double mutants, and so forth. TaM represents *Tyro 3<sup>-/-</sup>Axl<sup>+/-</sup>Mer<sup>-/-</sup>* mice. Average spleen weights ( $\pm$ SEM) are plotted for pooled male and female mice between 5 and 14 months of age;  $n = 3$  (TM), 4 (A, M, TaM), 5 (T), 6 (TA), 7 (AM), 8 (TAM), and 9 mice (WT). (D) FACS scans of expression of the B220 B cell marker versus the TCR $\alpha\beta$  T cell marker, in cells from wild-type (WT) and triple mutant (TAM) spleen and lymph node at 2 months of age. In these and all subsequent FACS scan panels, numbers in each quadrant are the percentage of cells in the sort that occupy that quadrant. (E) Expression of the T cell markers CD8 versus CD4 in WT and TAM spleen and lymph node at 2 months of age. (F) Colonies of small, darkly staining lymphocytes (arrows) in the liver, and in (G), the kidney, of a triple mutant. Bar, 0.1 mm.

## REPORTS

human autoimmune disorders, including rheumatoid arthritis (12) (Fig. 3A), pemphigus vulgaris (13) (Fig. 3B), and systemic lupus erythematosus (SLE) (14) (Fig. 3C). We detected recurrent thromboses and hemorrhage in several tissues, including the brain (Fig. 3D). These thromboses, which are associated with the presence of antibodies to phospholipids in human autoimmune syndromes (15), were especially prevalent in triple mutant females. Systemic autoimmune diseases result in elevated blood titers of antibodies directed against normal cellular antigens, including nucleoproteins and double-stranded (ds) DNA (16). Consistent with their autoimmune manifestations, we measured abnormally high levels of circulating antibodies to dsDNA throughout the allelic series of *Tyro 3* family mutants (17, 18) (Fig. 3E). In general, individuals carrying mutations in any two of the three genes exhibited higher  $\alpha$ -dsDNA titers than did single mutants; on average, triple mutant titers were the highest (Fig. 3E). Also prevalent were autoantibodies to various collagens (Fig. 3F), which are frequently detected in the sera of patients with rheumatoid arthritis (12). Circulating antibodies to phospholipids, which are among the most reliable indicators of human autoimmune syndromes characterized by recurrent thromboses, hemolytic anemia, and, in women, chronic infertility due to recurrent fetal loss (19), appeared throughout the allelic series. We detected markedly elevated antibody titers to cardiolipin (Fig. 3G), phosphatidylserine (11), phosphatidylethanolamine (11), and phosphatidylinositol (Fig. 3H). Elevated  $\alpha$ -cardiolipin titers were observed in several *Tyro 3* and *Axl* single mutants, and individual triple mutants frequently displayed titers that were 20- to 40-fold higher than wild type (Fig. 3G). Most triple mutant females never carried pregnancies to term.

B and T cells do not express the three receptor genes that we inactivated. Previous work has established that *Mer* is expressed by peripheral blood and bone marrow mononuclear cells, monocytes, and macrophages, but not by granulocytes or peripheral blood B or T lymphocytes (6, 20). Similarly, *Axl* is expressed by CD34<sup>+</sup> progenitor and bone marrow stromal cells and by peripheral monocytes and macrophages, but not by granulocytes or lymphocytes (21, 22). We used similar flow cytometric analyses with cell-specific markers to demonstrate that the *Tyro 3* gene is also the product of monocytes and macrophages but not of B or T cells (11). In addition, we used *in situ* hybridization to examine the sites of expression of the *Tyro 3*, *Axl*, and *Mer* mRNAs, and of the *Gas6* and *Protein S* mRNAs, in lymphoid tissues (Fig. 4, A through J). In the spleen, the mRNAs for all

three receptors and both ligands were localized to the red pulp and to the marginal zones, and were largely excluded from the periarteriolar lymphoid sheath, the B cell corona, and the germinal centers of the white pulp, which contain the bulk of both B and T cells (circled signal-free areas in Fig. 4, A, C, E, G, and I). The *Tyro 3* and *Axl* mRNAs were similarly absent from the primary lymphoid follicles and germinal centers of the lymph nodes (Fig. 4, B and D), which are predominantly composed of B cells, and the same was true for *Gas6* and *Protein S* (Fig. 4, H and J). Each of these mRNAs were instead localized to paracortical and medullary cord regions of the lymph node, which contain macrophages and T cells. A similar pattern was observed for *Mer* mRNA, although a small number of discrete *Mer*<sup>+</sup> cells were also detected within lymphoid follicles (Fig. 4F). The *Tyro 3*, *Axl*, and *Mer* mRNAs were each also confined to the central medulla of the

thymus (23), a localization that excludes expression by immature T cells but is consistent with expression by dendritic cells and macrophages.

In addition to these expression analyses, we performed a series of *in vivo* transfer experiments in both wild-type and triple mutant mice. We labeled wild-type spleen cells with the fluorescent dye carboxyfluorescein diacetate succinimidyl ester (CFSE) (24–26), which allowed us to measure the proliferation of the donor cells after injection. As measured by flow cytometry, successive rounds of cell division result in successive twofold diminutions in the fluorescence intensity of CFSE-labeled daughter cells. Three to 4 days after injection of CFSE-labeled cells, we analyzed spleens and lymph nodes of the injected mice for the number and fluorescence intensity of CFSE-labeled B220<sup>+</sup> B cells and of labeled CD4<sup>+</sup> and CD8<sup>+</sup> T cells (Fig. 4, K through N). As expected, injection of wild-type cells into wild-type recipients (WT →

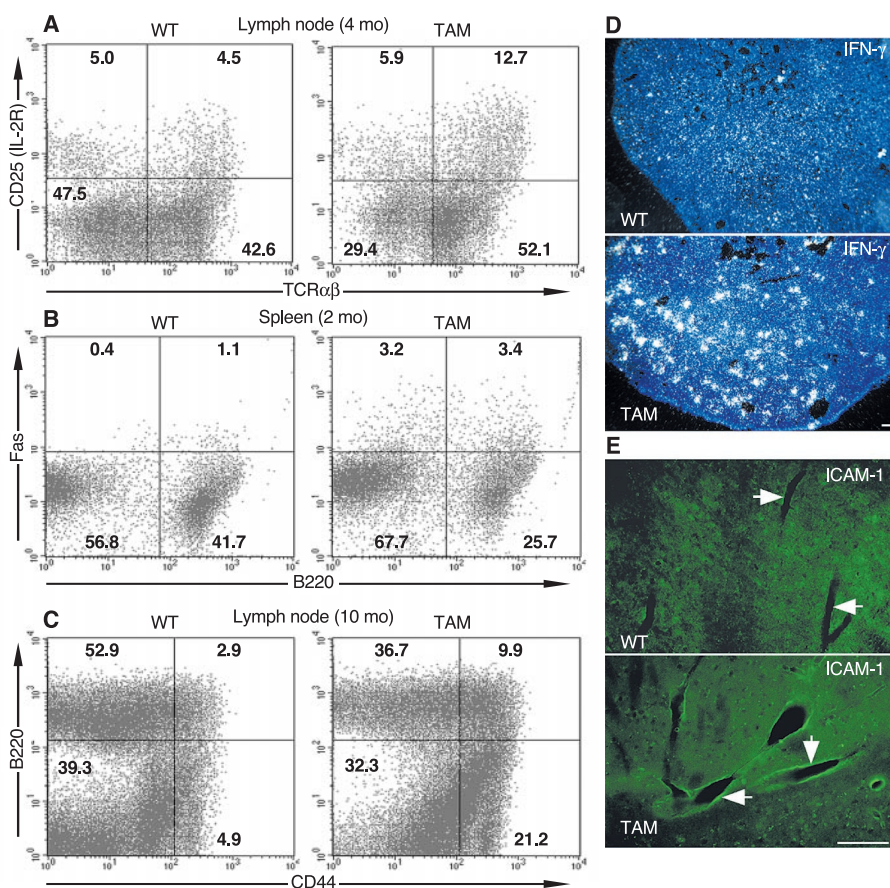


**Fig. 2.** Activation of the immune system in the triple mutants. (A) Expression of the IL-2 receptor (CD25) on TCR $\alpha\beta$ <sup>+</sup> nodal T cells from wild-type and triple mutant individuals at 4 months of age. (B) Expression of Fas on B220<sup>+</sup> splenic B cells from wild-type and triple mutant individuals at 2 months of age. (C) Expression of the chronic activation marker CD44 on B220<sup>+</sup> lymph node B cells from wild-type and triple mutant individuals at 10 months of age. (D) *In situ* hybridization to sections of lymph nodes from 6-month-old mice demonstrating strong up-regulation of IFN $\gamma$  mRNA in triple mutant (TAM) relative to wild type (WT). IFN- $\gamma$  mRNA is abundantly expressed in T cell-rich regions of the triple mutant spleen (17). (E) Immunohistochemical staining of ICAM-1 on endothelial cells lining blood vessels in the brain (arrows) in triple mutants (TAM) relative to wild type (WT). Bars, 0.1 mm.

REPORTS

WT) resulted in the recovery of nondividing B and T cell populations from the spleens and lymph nodes of the recipients (Fig. 4, L and N). In contrast, injection of the same cells

into triple mutants (WT → TAM) resulted in the recovery of wild-type donor B and T cells that had undergone multiple rounds of cell division. The wild-type B cells that failed to

proliferate in wild-type recipients were observed to undergo up to four rounds of cell division after 4.5 days in triple mutant spleens (Fig. 4K), and the wild-type T cells

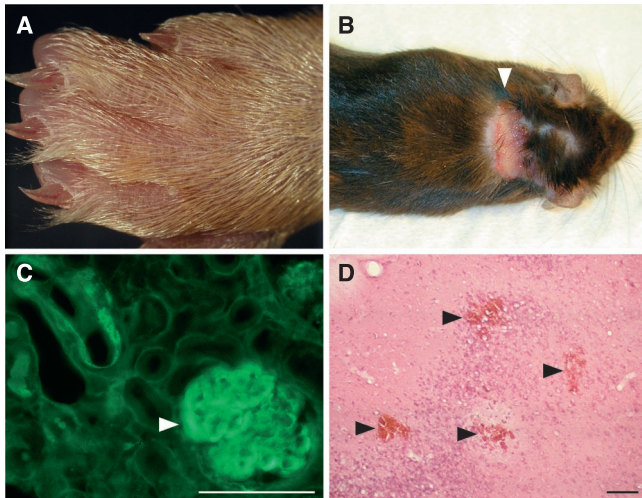


**Fig. 3.** Clinical and humoral manifestations of autoimmunity in *Tyro 3/Axl/Mer* triple mutants. (A) Swollen joints and footpad in a 6-month-old triple mutant female. Histologically, these symptoms were reflected in inflammation and lymphocyte invasion of the joints (17). (B) A typical skin lesion (arrowhead) on the upper back of an 8-month-old triple mutant female. (C) Immunoglobulin G (IgG) deposits in a glomerulus of the kidney (arrowhead) in a 12-month-old triple mutant female. (D) Blood vessel hemorrhages (arrowheads) in the brain of a 12-month-old triple mutant female. Bars, 0.1 mm. Circulating autoantibodies were measured in a 1:200 dilution of serum collected from single, double, and triple mutants of the *Tyro 3* allelic series, against dsDNA (E), collagen (F), cardiolipin (G), and phosphatidylinositol (H). Points represent the average of triplicate determinations by solid-phase ELISA (17, 18) in individual mice of the indicated genotypes. Genotype designations are as for Fig. 1C.

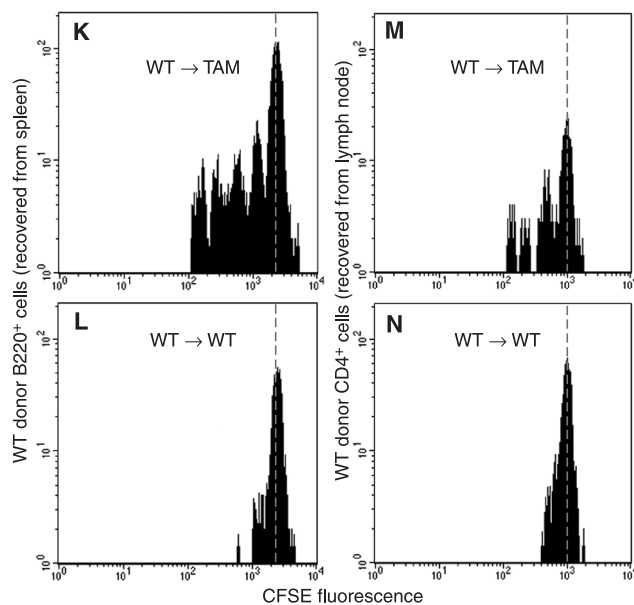
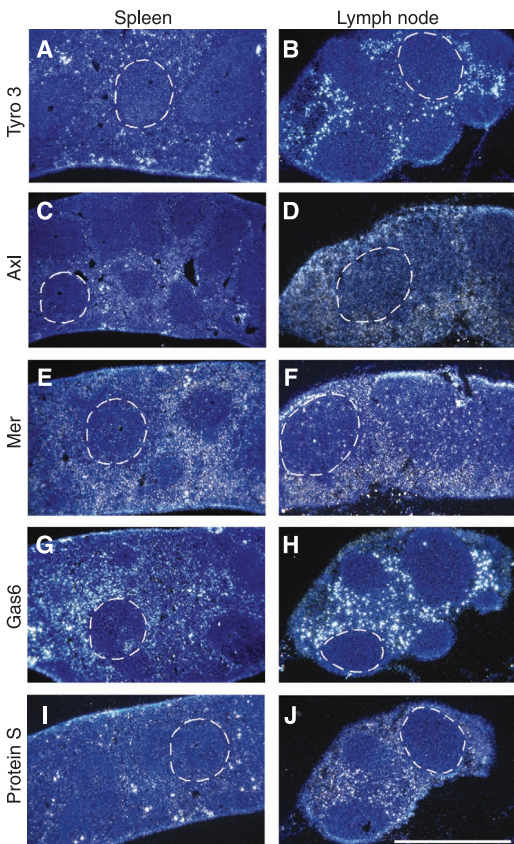
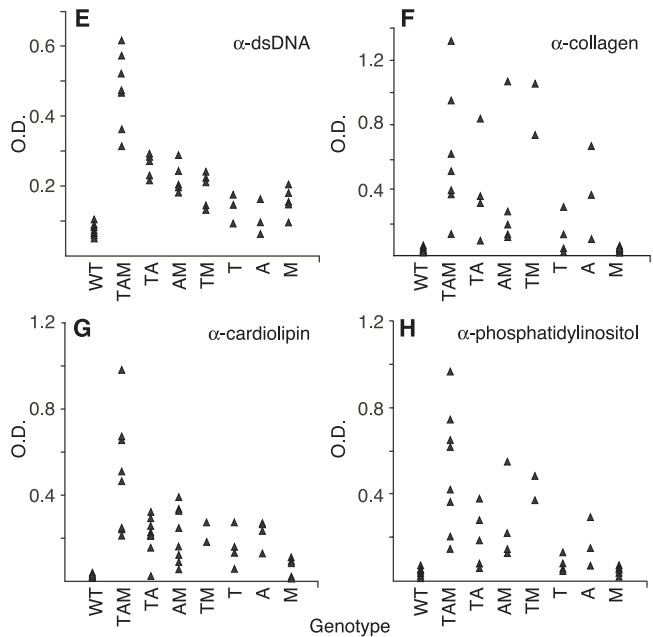


**Fig. 4.** Expression of the *Tyro 3* (A and B), *Axl* (C and D), *Mer* (E and F), *Gas 6* (G and H), and *Protein S* (I and J) mRNAs in lymphoid tissues. In situ hybridization was performed to sections of wild-type adult spleen (left column) and lymph node (right column). Dashed circles highlight signal-free areas in the white pulp of the spleen (left column) and lymphoid follicles of the lymph nodes (right column). Bar, 1 mm. See text for details. Host-dependent proliferation of wild-type B and T cells after transfer (K through N). Dissociated spleen cells from wild-type females at 2 (M and N) and 2.5 (K and L) months of age were labeled with CFSE (24–26), and injected into the tail veins of wild-type (L and N) and triple mutant (K and M) females at 8 to 10 months of age. Cells were recovered from either the spleens (K and L) or lymph nodes (M and N) of the recipients at 4.5 (K and L) and 4 (M and N) days after injection; dissociated cells were then analyzed by flow cytometry for expression of the B cell marker B220 (K and L) or the T cell marker CD4 (M and N) and were simultaneously measured for CFSE fluorescence intensity (x axis, all panels). Dotted lines mark mean CFSE fluorescence peaks that correspond to absence of proliferation of the injected cells.

## REPORTS

that failed to proliferate by 4 days after injection in wild-type recipients were observed to undergo up to three rounds of cell division by the same time in the triple mutant lymph nodes (Fig. 4M).

The above results suggest that rather than B and T lymphocytes, the cells that initiate the lymphoproliferation and autoimmunity of the *Tyro 3* family mutants are the macrophages and dendritic cells that normally express the three inactivated receptor genes. It has previously been noted that peritoneal macrophages cultured from *Mer* single mutants and challenged with bacterial lipopolysaccharide (LPS) express excessive levels of both activated nuclear factor kappa B (NF- $\kappa$ B) and the inflammatory cytokine tumor necrosis factor  $\alpha$  (TNF $\alpha$ ) (27, 28). Therefore, we examined the activation status of antigen-presenting cells (APCs) identified with the macrophage and dendritic cell markers CD11b and CD11c, at steady-state and in response to LPS stimulation, in triple mutants versus wild type (Fig. 5). Activated APCs

express elevated levels of major histocompatibility complex (MHC) antigens on their surface, and this was the case for APCs in the triple mutants. Although MHC class II (I-A<sup>b</sup>) levels were only modestly elevated in CD11c<sup>+</sup> cells freshly dissociated from triple mutant spleen or lymph node (Fig. 5A, upper panels), these levels were super-elevated in the same cells as an acute (1 hour) response to a 100 mg/kg intraperitoneal (IP) injection of LPS (Fig. 5A, lower panels). A similar LPS-induced super-elevation of the B7.2 (CD86) co-receptor, also a marker of APC activation, was observed (Fig. 5B). Triple mutant peritoneal macrophages expressed aberrantly high MHC class II levels in cell culture, even in the absence of LPS stimulation (Fig. 5C, upper panels), and these levels were even further elevated 5 hours after exposure to LPS (Fig. 5C, lower panels). We also observed that cultured triple mutant macrophages produced excessive amounts of the proinflammatory cytokine IL-12 (Fig. 5D), and exhibited a  $3.5 \pm 0.9$ -fold increase (rel-

ative to wild type) in generalized phagocytosis in vitro, as assayed by the uptake of fluorescently labeled *Escherichia coli* after 1 hour of co-culture (28, 29). Finally, serum levels of TNF $\alpha$  were  $11.3 \pm 2.5$  ng/ml 1 hour after injection of LPS into the triple mutants ( $n = 3$  mice), as compared to  $5.2 \pm 1.1$  ng/ml ( $n = 3$ ) for wild type.

The salient features of the autoimmune phenotypes described above have important implications for the development of autoimmunity in humans (23). The chronic hyper-activation of APCs in the triple mutants indicates that signaling through the *Tyro 3* family receptors normally serves as a self-extinguishing regulatory mechanism that limits the severity and time course of inflammatory immune responses. The frequently observed coexpression of the receptors and their ligands (9), together with the presence of conserved immunoreceptor tyrosine-based inhibition motifs (ITIM-like elements) (30) in the cytoplasmic domains of all three receptors, immediately suggest a molecular basis for this self-regulation (23), a model that we are currently testing.

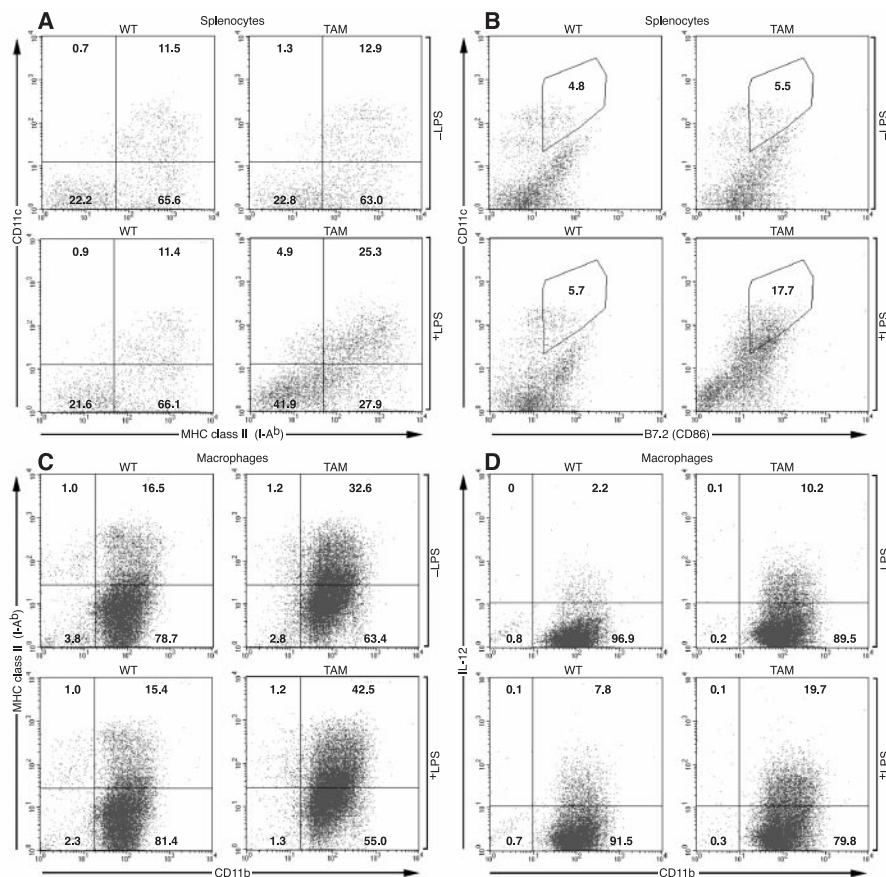


**Fig. 5.** Hyperactivation of APCs in the triple mutants. (A) Expression of MHC class II protein on the surface of CD11c<sup>+</sup> splenocytes isolated from wild-type (WT) and triple mutant (TAM) mice, before (-LPS) and 1 hour after (+LPS) an IP injection of LPS (100 mg/kg). (B) Expression of B7.2 on the surface of CD11c<sup>+</sup> splenocytes isolated from wild-type (WT) and triple mutant (TAM) mice, before (-LPS) and 1 hour after (+LPS) an IP injection of LPS. (C) Expression of MHC class II protein on the surface of wild-type (WT) and triple mutant (TAM) CD11b<sup>+</sup> peritoneal macrophages in culture, before (-LPS) and 5 hours after (+LPS) exposure to LPS (1  $\mu$ g/ml). (D) Expression of IL-12 in fixed and permeabilized wild-type (WT) and triple mutant (TAM) CD11b<sup>+</sup> peritoneal macrophages in culture, before (-LPS) and 5 hours after (+LPS) exposure to LPS.

### References and Notes

1. M. Lenardo *et al.*, *Annu. Rev. Immunol.* **17**, 221 (1999).
2. A. Miyajima *et al.*, *Annu. Rev. Immunol.* **10**, 295 (1992).
3. C. Lai, G. Lemke, *Neuron* **6**, 691 (1991).
4. C. Lai, M. Gore, G. Lemke, *Oncogene* **9**, 2567 (1994).
5. J. P. O'Bryan *et al.*, *Mol. Cell. Biol.* **11**, 5016 (1991).
6. D. K. Graham *et al.*, *Cell Growth Differ.* **5**, 647 (1994).
7. T. N. Stitt *et al.*, *Cell* **80**, 661 (1995).
8. P. J. Godowski *et al.*, *Cell* **82**, 355 (1995).
9. Q. Lu *et al.*, *Nature* **398**, 723 (1999).
10. Single-cell suspensions were prepared from lymphoid organs and depleted of red blood cells. Under conditions recommended by the antibody supplier,  $10^6$  cells were incubated with fluorescently labeled antibodies, and then washed three times with phosphate-buffered saline (PBS). Labeled cells were sorted on a Becton-Dickinson FACScan (fluorescence-activated) cell sorter. R-Phycoerythrin-, fluorescein isothiocyanate-, and cychrome-conjugated antibodies to CD45R/B220, CD4, CD8a, CD11b, CD69, CD44H, FAS, CD11c, TCR $\beta$  chain, I-A<sup>b</sup>, CD86, and IL-12 were purchased from BD Pharmingen. Conjugated antibodies to CD25 and ICAM-1 were purchased from Sigma and Chemicon, respectively.
11. Q. Lu and G. Lemke, unpublished data.
12. J. M. Stuart, A. S. Townes, A. H. Kang, *Annu. Rev. Immunol.* **2**, 199 (1984).
13. H. C. Nousari, G. J. Anhalt, *Lancet* **354**, 667 (1999).
14. B. H. Hahn, in *Dubois' Lupus Erythematosus*, D. J. Wallace, B. H. Hahn, Eds. (Williams & Wilkins, Baltimore, MD, 1997), pp. 69-75.
15. M. Greaves, *Haematologica* **84**, 32 (1999).
16. M. Z. Radic, M. Weigert, *Annu. Rev. Immunol.* **12**, 487 (1994).
17. D. C. Hess *et al.*, *J. Rheumatol.* **20**, 610 (1993).
18. Serum autoantibody levels to L- $\alpha$ -phosphatidyl-L-serine, L- $\alpha$ -phosphatidylinositol, L- $\alpha$ -phosphatidylethanolamine, L- $\alpha$ -cardiolipin, bovine collagen type II, and rat collagen type VII (all purchased from Sigma), and dsDNA, were measured in triplicate by enzyme-linked immunosorbent assay (ELISA), as described previously (17). For detection of dsDNA autoantibodies, salmon sperm dsDNA (100  $\mu$ g/ml in PBS) was added to poly-L-lysine-coated 96-well plates and dried overnight at room temperature. Coated wells were treated with SI-nuclease, and the ELISA was then continued as for the other antigens.

19. M. I. Bokarewa, M. Blomback, *Semin. Hematol.* **34**, 235 (1997).  
 20. D. K. Graham *et al.*, *Oncogene* **10**, 2349 (1995).  
 21. A. Neubauer *et al.*, *Blood* **84**, 1931 (1994).  
 22. A. Neubauer *et al.*, *Leuk. Lymphoma*, **25**, 91 (1997).  
 23. Web figure 1 and supplemental text are available at Science Online at [www.sciencemag.org/cgi/content/full/293/5528/306/DC1](http://www.sciencemag.org/cgi/content/full/293/5528/306/DC1).  
 24. A. B. Lyons, C. R. Parish, *J. Immunol. Methods* **171**, 131 (1994).  
 25. B. Ernst *et al.*, *Immunity* **11**, 173 (1999).  
 26. Single-cell suspensions were prepared by Ficoll-Paque gradient centrifugation of cells collected from 1-2 wild-type spleens. Cells were washed twice, resuspended in PBS/0.1% bovine serum albumin (BSA) at a concentration of  $1 \times 10^7$  cells/ml, and labeled with

CFSE (5  $\mu$ M) as described (24, 25). Labeled cells were adjusted to  $2 \times 10^7$ /ml, and 300  $\mu$ l of this suspension was injected intravenously into recipients' tail veins. Four to five days after injection, spleens and draining lymph nodes were collected, and single-cell suspensions were prepared for FACS sorting and analysis, as described above.  
 27. T. D. Camenisch *et al.*, *J. Immunol.* **162**, 3498 (1999).  
 28. R. S. Scott *et al.*, *Nature* **411**, 207 (2001).  
 29. Peritoneal macrophages were collected from 3% thioglycolate-treated mouse peritoneal cavities. After 2 hours of incubation in RPMI 1640 medium supplemented with 7% fetal bovine serum, unattached cells were washed off with culture medium and attached cells were cultured overnight. Phagocytosis assays were performed using a Vybrant Phago-

cytosis assay kit (Molecular Probes), as suggested by the manufacturer. Intracellular fluorescence at 520 nm was read on a Perkin-Elmer HTS7000plus bioassay reader.  
 30. M. Daéron, E. Vivier, *Curr. Topics Microbiol. Immunol.* **244**, 1 (1999).  
 31. The Tyro 3 mutants were originally generated in our lab by M. Gore (currently at Arena Pharmaceuticals), with the assistance of R. Klein and his colleagues (EMBL). We thank S. Goff, G. Matsushima, and H. Shelton Earp for providing the *Axl* and *Mer* single mutants and D. Littman and C. Surh for critical review of earlier versions of the manuscript. Supported by grants from the NIH.

17 April 2001; accepted 11 June 2001

## Regional Mu Opioid Receptor Regulation of Sensory and Affective Dimensions of Pain

Jon-Kar Zubieta,<sup>1,2\*</sup> Yolanda R. Smith,<sup>3</sup> Joshua A. Bueller,<sup>1</sup> Yanjun Xu,<sup>1</sup> Michael R. Kilbourn,<sup>2</sup> Douglas M. Jewett,<sup>2</sup> Charles R. Meyer,<sup>2</sup> Robert A. Koeppe,<sup>2</sup> Christian S. Stohler<sup>4</sup>

The endogenous opioid system is involved in stress responses, in the regulation of the experience of pain, and in the action of analgesic opiate drugs. We examined the function of the opioid system and  $\mu$ -opioid receptors in the brains of healthy human subjects undergoing sustained pain. Sustained pain induced the regional release of endogenous opioids interacting with  $\mu$ -opioid receptors in a number of cortical and subcortical brain regions. The activation of the  $\mu$ -opioid receptor system was associated with reductions in the sensory and affective ratings of the pain experience, with distinct neuroanatomical involvements. These data demonstrate the central role of the  $\mu$ -opioid receptors and their endogenous ligands in the regulation of sensory and affective components of the pain experience.

Considerable advances have been made in the understanding of pronociceptive mechanisms at the level of their transduction, transmission, and central nervous system representation (1-5). At supraspinal levels, the development and widespread utilization of functional neuroimaging has allowed the examination of changes in the metabolic function of brain regions during the experience of pain. These data have consolidated the view that pain is a complex experience encompassing sensory, affective, and cognitive elements. Neuronal nuclei engaged in its sensory perception and localization, as well as those involved in its anticipatory and affective components, have been described as a result (4-10). However, the function of the supraspinal antinociceptive systems regulating the pain experience has not been sufficiently

explored in humans. The existing data point to the presence of endogenous opioid release, a down-regulation of opioid receptors, or both, when patients diagnosed with persistent painful conditions have been studied before and after treatment with nonselective opioid receptor markers (11-13).

We examined the function of the endogenous opioid system and  $\mu$ -opioid receptors during the experience of sustained pain in healthy human subjects. The  $\mu$ -opioid receptors are implicated in antinociception, in stress-induced analgesia, and in the actions of exogenously administered opiate drugs (14-19). We studied 20 healthy volunteers, 13 men and 7 women, between the ages of 20 and 30 years (mean  $\pm$  SD,  $24 \pm 2$  years) (20) with positron emission tomography (PET) and [<sup>11</sup>C]carfentanil, a selective  $\mu$ -opioid receptor radiotracer (21, 22). Each volunteer was studied twice, during experimentally induced sustained pain and during placebo administration applied in the masseter (jaw) muscles. Placebo and sustained painful challenges were introduced 20 min after radiotracer administration and were maintained for 20 min. Pain intensity was maintained con-

stant (40 to 60 visual analog scale units) during that period of time (23). Pain and placebo conditions were administered in a double-blind, randomized and counterbalanced fashion. Parametric images of  $\mu$ -opioid receptor binding potential (defined as the  $B_{max}/K_d$  for this receptor site) were then produced using data obtained from 20 to 70 min posttracer administration (24). Pain intensity was rated every 15 s, and its sensory and pain-specific affective qualities were rated after completion of the PET scans with the McGill Pain Questionnaire (MPQ) (25). Each participant also received a high-resolution magnetic resonance imaging (MRI) anatomical scan (26) that was coregistered to the PET parametric images of receptor binding potential (27).

From prior work in experimental animals, it was hypothesized that the painful condition would be associated with an increased release of endogenous opioids in the anterior and ventrolateral portions of the thalamus contralateral to the painful challenge (28, 29), as well as in the ipsilateral amygdala (30). Under the experimental conditions used, the activation of the endogenous opioid system and  $\mu$ -opioid receptors would be observed as reductions in  $\mu$ -opioid receptor availability in vivo as measured with PET during the sustained pain condition, compared with placebo. Significant activations of the  $\mu$ -opioid receptor system were detected in volumes of interest selected in the amygdala ipsilateral to the painful stimulus and in the contralateral ventrolateral portion of the thalamus. These data supported the initial hypothesis that the presence of sustained pain would induce a regionally selective release of endogenous opioids interacting with  $\mu$ -opioid receptors, resulting in either competition with the radiolabeled tracer for the receptor sites, receptor internalization and recycling, or both (Table 1). The lateralization of these effects is also consistent with those observed in experimental animals (28, 30).

In a second analysis, differences between pain and placebo conditions were tested for statistical significance on a pixel-by-pixel basis using statistical parametric mapping tech-

<sup>1</sup>Department of Psychiatry and Mental Health Research Institute, <sup>2</sup>Department of Radiology, <sup>3</sup>Department of Obstetrics and Gynecology, Medical School, and <sup>4</sup>Department of Biologic and Materials Sciences, School of Dentistry, The University of Michigan, Ann Arbor, MI 48104-1687, USA.

\*To whom correspondence should be addressed. E-mail: [zubieta@umich.edu](mailto:zubieta@umich.edu)